Eur. Phys. J. D **25**, 149–155 (2003)
DOI: 10.1140/epjd/e2003-00239-9

THE EUROPEAN PHYSICAL JOURNAL D

Study of the structural photoinduced dynamics of a solid Kr matrix with an NO impurity

J.C. Castro Palacios[1,a], L. Velazquez[1,b], G. Rojas-Lorenzo[2,c], and J. Rubayo-Soneira[2,d]

[1] Departamento de Física, Universidad de Pinar del Río, Martí 270, Esq. 27 de Noviembre, Pinar del Río, Cuba
[2] Departamento de Física General y Matemáticas, Instituto Superior de Ciencias y Tecnología Nucleares Quinta de los Molinos, Ave. Carlos III y Luaces, Plaza C. Habana, Cuba

Received 13 October 2002 / Received in final form 27 February 2003
Published online 30 July 2003 –

Abstract. In the present work we studied the immediate medium response to the excitation to the $A(3s\sigma)$ Rydberg state of NO impurity embedded in a solid Kr matrix. The excitation, extended over a large range of the lattice was investigated by classical molecular dynamics simulations. This has been done using Lennard-Jones pair potentials from the literature for the NO($X^2\Pi$)−Kr interactions and fitted in this work for the NO($A^2\Sigma^+$)−Kr ones, since these last have not been reported in literature. Thus is obtained the first shell response to the excitation of the impurity (approximately the first 2 ps) as well as the response of the continuous shells up to the 10th one. This first response of the first shell is compared to that for similar systems (Ne and Ar matrixes doped with NO). Therefore some theoretical conclusions are drawn. The results indicate the inertial character of the response propagation throughout the surrounding medium and the high degree of nuclear coherence at short times.

PACS. 34.30.+h Intramolecular energy transfer; intramolecular dynamics; dynamics of van der Waals molecules – 02.70.Ns Molecular dynamics and particle methods – 31.70.Ks Molecular solids

1 Introduction

The many-body dynamics in response to photoexcitation in condensed media is of general interest in many systems, such as: biological molecules, condensed phase chemical media and solids (insulators and semiconductors [1]). Extensive configurational rearrangements following photoabsorption are observed in such systems. Pure and doped rare gas solids have long been considered as good model systems for describing and understanding the basic principles behind such a medium response [2–4]. They result amenable to modelization because of their simple structural properties and the great knowledge of their physical properties. To this respect, molecular dynamics simulations have been used to describe simple photochemical reactions during this decade in rare gas liquids [5–8], solids [4,7,9–12] and clusters [9,10,13,14]. Such events are driven by the photoinduced intramolecular motion which induces nuclear dynamics of the surrounding cage [11,15, 16], as well as long range propagation of energy [16–18].

It is known that excitation of low-n Rydberg states of impurity molecules or atoms in rare gas solids leads to a large blue spectral shift in absorption, as compared to the gas phase, due to the strong short range repulsion between the Rydberg electron and the closed shell of rare gas atoms [2,19]. The strong repulsion leads to a relaxation of the cage species surrounding the excited center to a new equilibrium configuration from which fluorescence occurs. The large absorption-emission Stokes shifts that are observed reveal the extensive lattice rearrangements around the excited species. The basic mechanism is considered to be a radial expansion of the cage (the so-called electronic "bubble" formation) [1,2,19,20] which is also operative in rare gas liquids and clusters [1,2,21].

In the case of rare gas van der Waals solids, cage relaxation upon Rydberg state excitation of impurities has been intensively studied over the past few years [2,4,19,20, 22–25]. Chergui *et al.* have mainly investigated the case of NO-doped rare gas solids [4,19,24,26] and H_2 solids [4,22,25].

However, combining molecular dynamics (MD) simulations and a normal mode analysis a better study can be done. Jiménez *et al.* [27,28] have developed computer simulations to study the dynamics of structural relaxation in Rydberg excited NO-doped Ar crystals. They have reasonably described the experimental results for the Stokes

[a] e-mail: juanc@geo.upr.edu.cu
[b] e-mail: luisberis@geo.upr.edu.cu
[c] e-mail: german@fctn.isctn.edu.cu
[d] e-mail: jrs@fctn.isctn.edu.cu

shift and the bubble size [19,26] as well as some insights in the ultrafast dynamics of structural relaxation around the impurity after excitation. These results showed a behavior characterized by an impulsive expansion of the cage radius at short times (≤ 250 fs), followed by multimodal oscillations over several picoseconds around a radius of ~ 4 Å. This corresponds to a dilatation of the ground state cage radius by $\sim 10\%$. The first shell of atoms around the impurity has an inertial character in its response to the excitation of the NO molecule in the initial 100−150 fs. Similar behavior was found by Vigliotti *et al.* [29] when studying NO-doped Ne crystals. They also applied MD simulations, and the results for this matrix showed that the cage radius expands much more than in Ar–NO systems and also that the cage radius compresses back (medium response to photoexcitation) more slowly (~ 1400 fs), what is in good accordance with experimental results (see [19,26,29]).

Our work constitutes a starting point for the theoretical study of a new and interesting system, NO-doped Kr crystals, by means of molecular dynamics simulations. The motivation of this work is to study the immediate response of the Kr matrix to the excitation of the NO impurity in comparison to similar more studied systems such as: Ar and Ne matrixes doped with NO ([27,28] for Ar–NO and Vigliotti *et al.* [29] for Ne–NO). For this purpose we attempted to implement a new approach to the potential parameters in order to describe the NO($A^2\Sigma^+$)–Kr interactions, so as to be able to run simulations, and thus make a comparative theoretical study of the dynamical behavior of the Kr medium in response to photoexcitation.

The outline of the paper is the following: in Section 2 we show the methodology for modelling the interactions between the species and for the dynamics. In Section 3 we present the results and discussions, and finally some conclusions are drawn in Section 4.

2 Methodology

2.1 Intermolecular potentials

In our work we modeled the interactions between the species by using Lennard-Jones (L-J) pair potentials. These potentials have the following mathematical form:

$$V(R_{ij}) = \epsilon_{ij}\left[\left(\frac{\sigma_{ij}}{R_{ij}}\right)^6 - \left(\frac{\sigma_{ij}}{R_{ij}}\right)^{12}\right]. \qquad (1)$$

with $R_{ij} = \|r_j - r_i\|$, where ϵ_{ij} and σ_{ij} are the L-J parameters and R_{ij} is the intermolecular distance between the particles i and j.

The L-J potential parameters for the Kr–Kr and NO($X^2\Pi$)–Kr interactions were taken from literature ([30,31], respectively), see Table 1.

The L-J potential parameters for the NO($A^2\Sigma^+$)–Kr interactions used in this work were fitted by using Molecular Dynamics (MD) simulations since they have not been reported yet. This was accomplished by finding the best values of σ_{ij} and ϵ_{ij} reproducing the available spectroscopic data for the studied system: Stokes shift and absorption-emission energies [19]. This methodology yielded the parameters registered in Table 1. The calculated values that match the experimental results for the used parameters are indicated in Table 2. It can be seen that there is a great agreement to the Stokes shift in the fit, which is directly related with the nature of the potentials. More details about the molecular dynamics simulation used to fit the parameters above can be found in Section 2.2.

Table 1. L-J potential parameters for the Kr–Kr, NO($X^2\Pi$)–Kr and NO($A^2\Sigma^+$)–Kr (fitted in this work) interactions.

	σ_{ij} (Å)	ϵ_{ij} (eV)
Kr–Kr	3.65	0.01404
NO($X^2\Pi$)–Kr	3.68	0.01437
NO($A^2\Sigma^+$)–Kr	4.25	0.01084

Table 2. Spectral energy results obtained by the simulation using L-J fitted parameters for the NO($A^2\Sigma^+$)–Kr interactions in comparison to the available experimental measurements. *Eab* is the absorption energy and *SS* the Stokes shift.

	Eab (eV)	*SS* (eV)
calculated	5.97	0.350
experimental [19]	6.08	0.380

We used L-J pair potentials to model the NO($A^2\Sigma^+$)–Kr interactions due to the fact that these potentials have a good mathematical form suitable for this purpose and on the other hand we have the previous works developed by Jiménez *et al.* [27,28] on the NO-doped Ar matrix Missing system, which give similar results to ours.

It was shown for the case of NO-doped Ar matrixes [28] that the dynamics for that system can be reproduced in the same way by using L-J pair potentials or by using repulsive Born-Mayer potentials for the NO($A^2\Sigma^+$)–Kr interactions, but only one thing must be taken into account: these potentials must have the same asymptotic behavior in the repulsive zone. We also checked the above aspect for the studied system. We fitted a Born-Mayer potential,

$$V(r) = A\exp\left(-\left(\frac{r - r_0}{b}\right)\right), \qquad (2)$$

with $A = 3000$ cm^{-1}, $r_0 = 3.5$ Å and $b = 0.2$ Å. We corroborated this idea one more time proving that the same first shell response is obtained after the excitation of the impurity (see Fig. 4) and it was also detected that the NO molecule receives the same influence of the lattice for both potentials (see Sect. 3). All this has been tested taking into account the conditions stated above for Lennard-Jones and Born Mayer potentials in the repulsive zone.

L-J potentials are used to obtain the results of this work. When Born-Mayer potentials are used it will be aforementioned.

2.2 Molecular dynamics

The methodology of the simulation has been very well commented in references [27,28]. Even so, for a rapid understanding of it, we believe it is important to recall some aspects. The simulated system consists of a face centered cubic (fcc) supercell structure with 499 atoms and an NO molecule placed at a substitutional site. Periodic boundary conditions are used to simulate an infinite crystal. The size of supercells contains 10 shells of independent neighbors corresponding to 200 particles.

At the experimental temperature $T = 4$ K the zero-point motion dominates the nuclear motion of the Kr atoms. A scaled temperature approach was used to model the system ([4,32]):

$$T' = \frac{\hbar\omega_{\mathrm{D}}}{2k_{\mathrm{B}}}\left(\tanh\left(\frac{\hbar\omega_{\mathrm{D}}}{2k_{\mathrm{B}}T}\right)\right)^{-1}, \qquad (3)$$

with $\omega_{\mathrm{D}} = 50\ \mathrm{cm}^{-1}$ being the Debye frequency of solid Kr. According to the values, the new effective temperature for the thermalization system was $T = 36$ K. This temperature approach has been previously used [11,27,28] with satisfactory results.

To realize the simulation we followed these steps:

1. the atomic positions were altered by random shifts of the atoms and the initial velocities were given in order to make zero the total initial momentum;
2. the system was thermalized in the ground state of the NO molecule. An effective temperature of $T = 36$ K was used;
3. following the above steps we arrived at an initial configuration (positions and velocities) for the integration of trajectories in the microcanonical ensemble. The next step was to make the numerical integration of a system of $N = 500$ interacting particles described by Hamiltonian presented in [27,28];
4. to calculate the spectroscopic data the vertical transition was simulated by an instantaneous change of the ground state potential energy surface for the excited one;
5. the medium response after excitation of the NO molecule was visualized by following the temporal evolution of the different shell radii given by the expression:

$$R_n(t) = \frac{1}{N_n}\sum_{j=1}^{N_n}\left\|r_n(t) - r_{\mathrm{NO}^*}(t)\right\|, \qquad (4)$$

that is the mean distance between the NO($A^2\Sigma^+$) molecule and the nth surrounding shell of Kr atoms (containing N_n atoms).

By means of the above simulation we described the NO–Kr interactions and ran the dynamics of the system, through the fitting of the L-J potential parameters.

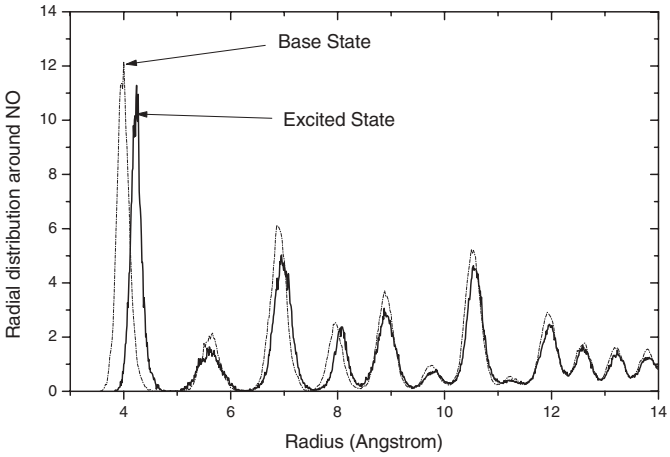

Fig. 1. Radial distribution function of the NO-doped Kr crystal in the ground and excited state respectively.

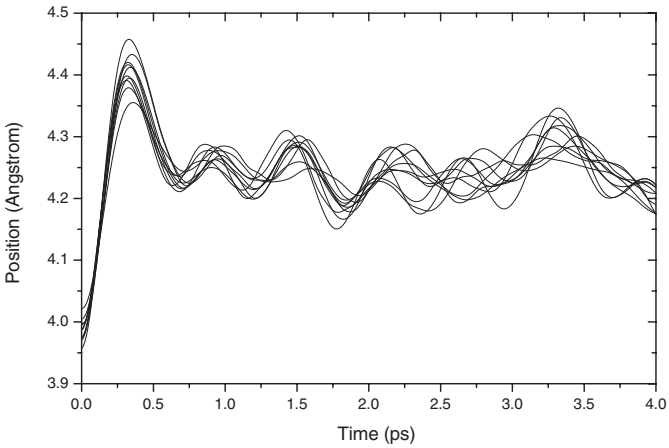

Fig. 2. Individual trajectories of the 12 atoms of the first shell around the NO impurity. What plotted is the NO–Ar distance.

3 Results and discussions

The radial distribution function of a NO-doped Kr crystal in the ground state is given in Figure 1. We considered not to show that corresponding to the pure crystal because it almost perfectly overlaps it. So, we can say that the substitution of a Kr atom by the NO molecule hardly affects the lattice. This is a direct consequence of the similarity of Kr–Kr and NO($X^2\Pi$)–Kr pair potentials (Tab. 1).

The large absorption gas-to-matrix shift characterizes the strong short-range repulsion between the excited NO molecule and its environment. The consequence of this repulsion is a structural relaxation whose signature is the Stokes shift.

By using the expression given in equation (4) for the first shell we obtained the individual trajectories shown in Figure 2. An oscillatory multimode evolution of $R_1(t)$ (mean first shell radius), and a high degree of nuclear vibrational coherence could be noticed. These trajectories remain bundled together during the dynamics. It is more

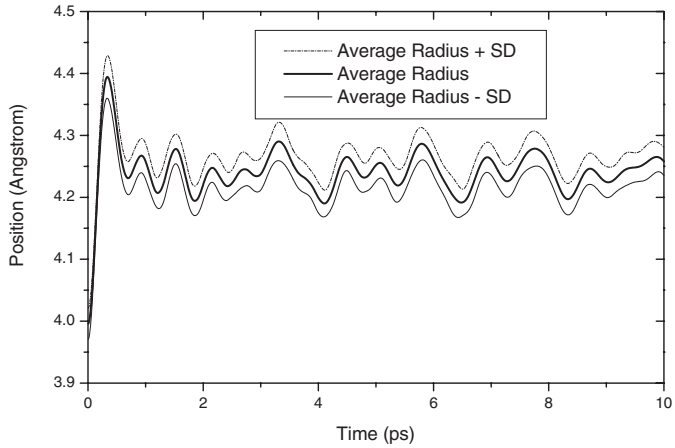

Fig. 3. Average of 100 individual trajectories of the first shell average radius plus (and minus) the standard deviation (SD) at every point.

stressed in the first 330 fs, deriving fairly similar responses for the 12 atoms of this shell.

An average of 100 individual trajectories is shown in Figure 3, along with the $R_1(t) + \sigma$ (standard deviation) and $R_1(t) - \sigma$ curves. Once again, it can be seen the high degree of spatial coherence of the first shell atoms, mainly within the first 330 fs.

We can also appreciate in Figure 3, two time regimes: one at short time and another at long time periods. The first is characterized by an impulsive increase of the cage radius from 4.01 Å (which corresponds to the equilibrium NO–Kr distance in the ground state) to 4.39 Å, that takes place in about 330 fs. This expansion of the cage radius results from the strong repulsion between the Rydberg excited molecule and the surrounding Kr atoms. The perturbation induced in the crystal by the excited NO molecule displaces the Kr atoms far from equilibrium. After 330 fs, the motion of the Kr atoms in the first shell is reversed due to their interactions with the next shells of atoms and the cage compresses back to a radius of 4.23 Å in $\sim$ 690 fs. If we compare, in this sense, our system with the NO-doped Ar matrix and the NO-doped Ne matrix, it can be seen that the first compresses back in $\sim$ 800 fs [33] and the second one in $\sim$ 1400 fs [29], that is, in the case of Ne matrixes it takes much longer. This should be called to attention since Ne atoms are less heavy than Kr and Ar atoms and Ne–Ne distances are also smaller. This matrix could be expected to have a faster response than Kr and Ar matrixes, but in reality that is not the case. For assessing a theoretical explanation of this behavior two factors must be taken into consideration: the potentials (ground and excited state) and the mass of the matrix atoms. After the excitation of the NO impurity the excited state pair potentials (NO($A^2\Sigma^+$)–(Kr, Ar, Ne)) provoke a very strong repulsion of the shells around the impurity. In the case of Ne matrixes some shells besides the first one are affected (up to the third shell), due to the little resistance of the matrix, the first shell expands more than in Kr and Ar matrixes. The parameter ε_{ij} of Ne–Ne interactions is the weakest of the three (see Tab. 3) and therefore the Ne atoms can be more easily shifted from their equilibrium positions. On the other hand, Kr and Ar matrixes show similar potentials for Kr–Kr and Ar–Ar interactions. This fact also makes similar the lattice constant ($a_{\mathrm{Kr}}/a_{\mathrm{Ar}} \sim 1.06$). For both systems the excited potential moves only the first shell, resulting for the Kr matrix, the greatest mass displacement ($m_{\mathrm{Kr}}/m_{\mathrm{Ar}} \sim 2$). In this situation, the deciding criterion aims at the cage effect, which is more stressed in the Kr matrixes (ϵ_{ij} has the greatest value of the three, see Tab. 3). As a result of all this, the Kr matrix atoms have the least increase of the first shell after the excitation of NO as compared to the Ne and Ar first shell atoms [19] and also the faster first contraction of the first shell (medium response).

Table 3. Lennard-Jones potential parameters for Ne–Ne, Ar–Ar and Kr–Kr interactions.

	σ (Å)	ϵ (eV)
Ne–Ne [30]	2.74	0.00310
Ar–Ar [30]	3.40	0.01040
Kr–Kr [30]	3.65	0.01404

The above ultrafast response is followed by a complex oscillatory pattern around the average NO–Kr distance of $\sim$ 4.24 Å, which is the equilibrium cage radius in the Rydberg state. The amplitude of the oscillations is damped in the course of time. The size of the cage radius of $\sim$ 4.24 Å in the Rydberg state corresponds to an increase of $\sim$ 6% of the initial cage radius, 4.01 Å. This data is in accordance with the experimental results for the bubble size for these systems [19], which refer that it varies increasing in order of mass from Xe–NO ($\sim$ 3%), Ar–NO ($\sim$ 10%) to Ne–NO ($\sim$ 15%). The experimental result for Kr–NO doped matrix is not published, but it can be easily seen that it fulfills the former criterion with a value of $\sim$ 6%.

In Figure 4, we compare the average radius of the first shell *versus* time for both the L-J potential and for Born-Mayer potential (B-M). The response is essentially the same. This suggests that the dynamics is largely driven by short range repulsive forces, the attractive part of L-J potentials being unimportant. We also tested the influence of the lattice on the NO molecule for each potential. We took an excited state equilibrium lattice (it is the same for both potentials) and we checked the potential well of the NO molecule by varying the average first shell radius around its equilibrium position $\sim$ 4.24 Å *versus* the total potential energy. In this zone, these two pair potentials have different signs but the resulting addition of all the interaction over the 500 atoms yields the same stable configuration for the NO potential well in both cases. It is also important to point out that the NO($A^2\Sigma^+$)–Kr interactions do not contribute very much to the total potential energy in comparison to the Kr–Kr interactions. These results showed that both potentials (B-M and L-J) used to describe the NO($A^2\Sigma^+$)–Kr interactions are equivalent in the matrix.

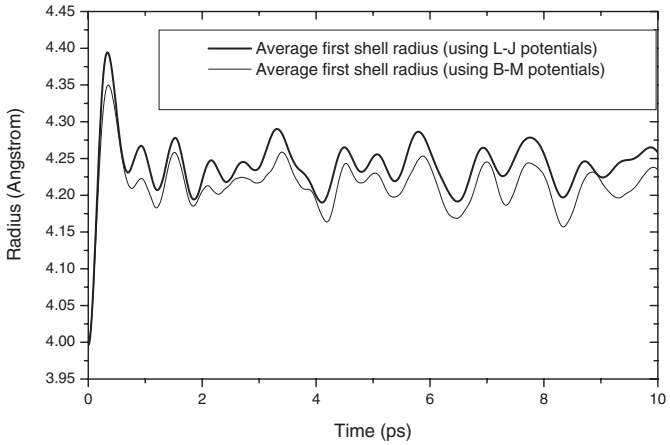

Fig. 4. Time evolution of the first shell radius in the case of Lennard-Jones potentials (thick line) and of Born-Mayer potentials (thin line) for the NO*–Kr interactions. The traces are an average of 100 trajectories each.

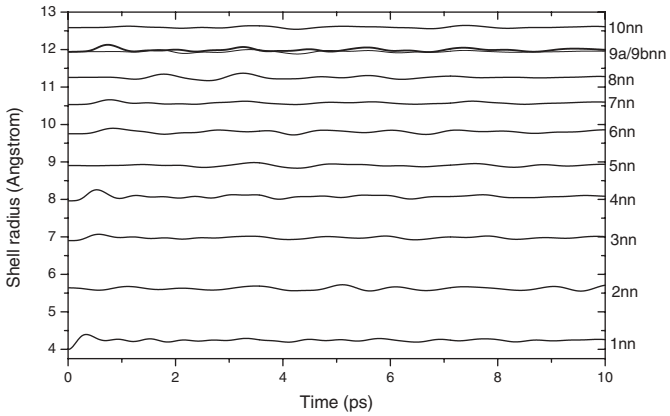

Fig. 5. Time evolution of the radii of the ten shells around the NO impurity. The trajectory of the 9th *a* shell radius is shown by a thick line, whereas that of the 9th *b* is shown by a thin line.

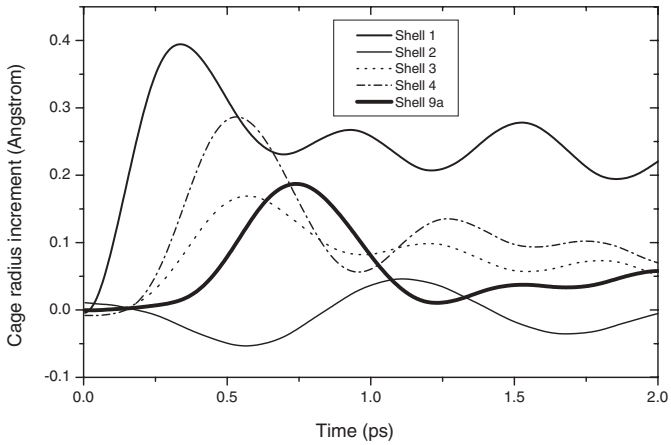

Fig. 6. Time evolution of the radius increment for the first four shells and of the 9th *a* in the first 2 ps after excitation.

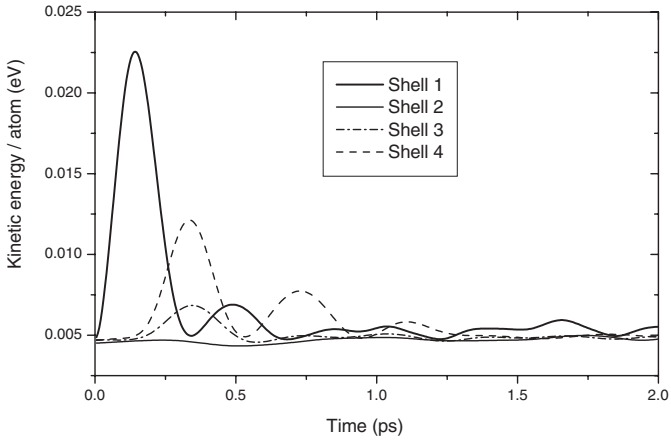

Fig. 7. Time evolution of the kinetic energy per atom for the first four shells in the first 2 ps after excitation.

For the case of the higher shells, Figure 5 shows the average cage radius over 100 individual trajectories for all the coordination shells around the impurity up to the tenth. The 9th shell is divided into two subshells: the 9th a shell that contains the atoms located on the (110) crystallographic axis, the same that includes the positions of the impurity and the first and fourth shell of Kr atoms; and the 9th *b*, that contains the atoms located in the (411) axis. It is easy to see that the 1st, 4th, and 9th *a* shells are those that undergo the largest displacements at early time periods. The 3rd, 6th, and 7th shells respond mildly, while the rest hardly respond, although they lie closer to the first shell, such as: the 2nd or 5th one. The largest radius increments occur for the 1st (~ 0.22 Å) and the 4th (~ 0.11 Å) shells.

From the onset of the response of the 1st, 4th, and 9th a shells in Figure 5, we estimated the propagation velocity of the resulting deformation to be $\sim 1922 \pm 180$ m/s. The longitudinal velocity of sound in solid Kr is ~ 1370 m/s [20], implying that the deformation travels at a slightly supersonic velocity. If we compare with the results obtained by Jiménez *et al.* [27] for NO-doped Ar matrix: $\sim 2750 \pm 250$ m/s of propagation velocity, a clear shock wave, being the longitudinal velocity of sound in solid Ar ~ 1600 m/s, it can be seen that for the Kr matrix it is lower. On the other hand, the longitudinal velocity of sound in Ne matrixes is ~ 1130 m/s [20].

Figure 6 shows the time evolution of the radii of the first four shells and of the 9th a shell. We observed that the first shell increases its radius up to 170 fs while the rest have not moved yet. Conversely, it can be appreciated in Figure 8 that the potential energy of the first shell atoms drastically drops from its initial value in ~ 160 fs. Over the same time scale, this potential energy is entirely converted to kinetic energy (Fig. 7). The complete conversion of potential energy into kinetic energy in the first ~ 160 fs clearly shows the adiabatic character of the first shell expansion over this time.

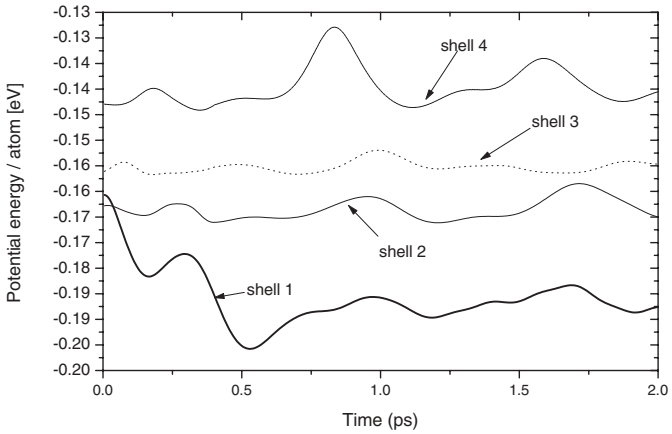

Fig. 8. Time evolution of the potential energy per atom for the first four shells in the first 2 ps after excitation.

For times beyond ~ 160 fs the deformation exerted on the 3rd and 4th shells leads to an increase of their potential energy which rises and falls at later times. This increase is larger for the 4th shell. The energy exchange between shells can be seen in this behavior of the kinetic energy (Fig. 7). The first shell reaches a maximum value at ~ 160 fs, and then falls near to zero by ~ 340 fs. Another maximum can also be detected at ~ 490 fs. This maximum drops near to zero by ~ 650 fs. It is clear from this behavior that there is an interchange of energy between the first shell and the others. This last aspect can also be appreciated when observing that the 3rd and 4th shells reach their maximum kinetic energy as the first shell experiences its first minimum.

The molecular dynamics simulations of the higher shells reveal a high degree of directionality of the deformation propagation in the solid (Fig. 5). This directionality is determined by the geometry of the first shell of Kr atoms around the impurity. These atoms and the impurity define the (110) crystallographic axis of the crystal, along which, the deformation is preferentially propagated.

4 Conclusions

In this work we realized the study of the NO-doped krypton matrix response after excitation of NO. We focused mainly on the immediate response of the shells around the NO impurity. In that sense, fitted L-J potentials are used to model the NO($A^2\Sigma^+$)–Kr interactions. It was observed that there is a high degree of nuclear coherence in the first 330 fs. The average radius of the first shell showed an increase after excitation of $\sim 6\%$ which is in good accordance with experimental results [19] (between 3% and 9%). The inertiality of the first shell response is very well appreciated. It expands up to 170 fs without any answer of the other shells. The adiabatic character of the first expansion at short periods and the interchange of energy among the shells is also noticed. There is a clear dependence of the response propagation on the crystallographic direction in the lattice. This is appreciated when the case of the 1st, 4th and 9th a shells, which are directionally connected, is compared with the case of the other shells. A great part of the energy is transmitted in the geometrically connected shells direction. Similar behavior of the medium response after excitation of the impurity was also observed by Jiménez *et al.* [27,28] for the case of NO-doped Ar matrixes. On the other hand, we were able to realize that the cage compresses back to a radius of 4.23 Å in ~ 690 fs. This result showed that the Kr matrix responds much faster than the Ne matrix (1400 fs) [29] to the excitation of the NO impurity and slightly slower than the Ar matrixes (800 fs) [33]. This order in the responses can be attributed to the nature of potentials (ground and excited state) as well as the mass of the matrix atoms.

We would like to thank to Prof. M. Chergui for his fruitful discussion and suggestions. This work has been supported by a supply from a DAAD project directed by Prof. Mario Piris from the ISCNT, Havana, Cuba.

References

1. J. Jortner, in *Femtochemistry, Ultrafast Chemical and Physical Processes in Molecular Systems*, edited by M. Chergui (World Scientific, Singapore, 1996), p. 15
2. N. Schwentner, E.E. Koch, J. Jortner, *Electronic Excitation in Condensed Rare Gas Solids* (Springer, Berlin, 1985)
3. V.E. Bondybey, Adv. Chem. Phys. **41**, 269 (1980)
4. N. Schwentner, V.A. Apkarian, Chem. Rev. **99**, 1481 (1999)
5. I. Benjamin, K.R. Wilson, J. Chem. Phys. **90**, 4176 (1989)
6. Q.L. Liu, C. Wan, A.H. Zewail, J. Chem. Phys. **100**, 18666 (1996)
7. A.I. Krylov, R.B. Gerber, J. Chem. Phys. **100**, 4242 (1994)
8. V.E. Batista, D.F. Coker, J. Chem. Phys. **105**, 4033 (1996)
9. R. Alimi, R.B. Gerber, V.A. Apkarian, J. Chem. Phys. **89**, 174 (1998); R. Alimi, V.A. Apkarian, R.B. Gerber, J. Chem. Phys. **98**, 331 (1993)
10. R.B. Gerber, A.I. Krylov, *Reaction Dynamics in Clusters and Condensed Phase*, edited by J. Jortner *et al.* (Kluwer Academic Publishers, Netherlands, 1994), p. 509
11. R. Zadoyan, Z. Li, C.C. Martens, V.A. Apkarian. J. Chem. Phys. **101**, 6648 (1994); Z. Li, R. Zadoyan, V.A. Apkarian, C.C. Martens, J. Phys. Chem. **99**, 7435 (1995)
12. I.H. Gersonde, H. Gabriel, J. Chem. Phys. **98**, 2094 (1993); I.H. Gersonde, S. Hennig, H. Gabriel, J. Chem. Phys. **101**, 9558 (1994)
13. F.G. Amar, B.J. Berne, J Chem. Phys. **88**, 6720 (1984); L. Perera, F.G. Amar, J. Chem. Phys. **90**, 7354 (1989)
14. Q. Liu, J.-K. Wang, A.H. Zewail, Nature **364**, 427 (1993); J.-K. Wang, Q. Liu, A.H. Zewail, J. Phys. Chem. **99**, 11321 (1995)
15. Z. Li, J.Y. Fang, C.C. Martens, J. Chem. Phys. **104**, 6919 (1996)
16. A. Goldberg, J. Jortner, J. Chem. Phys. **107**, 8994 (1997)
17. S. Cui, R.E. Jhonson, P. Cummings, Surf. Sci. **207**, 186 (1988)
18. A. Borrman, C.C. Martens, J. Chem. Phys. **102**, 1905 (1995)

19. M. Chergui, N. Schwentner, V. Chandrasekharan, J. Chem. Phys. **89**, 1277 (1988)
20. I.Ya. Fugol, Adv. Phys. **37**, 1 (1978)
21. J. Wörmer, R. Karabach, M. Joppien, T. Möller, J. Chem. Phys. **104**, 8269 (1996); O. Bjorneholm, F. Federmann, F. Fösing, T. Möller, Phys. Rev. Lett. **74**, 3017 (1995); O. Bjorneholm, F. Federmann, F. Fösing, T. Möller, S. Stampfli, J. Chem. Phys. **104**, 1876 (1996); M. Lengen, M. Joppien, R. von Pietrowski, T. Moller, Chem. Phys. Lett. **229**, 362 (1994)
22. F. Vigliotti, M. Chergui, M. Dickgiesser, N. Schwentner, Faraday Discuss. **108**, 139 (1997)
23. J. Goodman, L.E. Brus, J. Chem. Phys. **67**, 933 (1977); **69**, 4083 (1978)
24. M.T. Portella-Oberli, C. Jeannin, M. Chergui, Chem. Phys. Lett. **259**, 475 (1996)
25. C. Jeannin, M.T. Portella-Orbeli, F. Vigliotti, M. Chergui, Chem. Phys. Lett. **279**, 65 (1997)
26. M. Chergui, N. Schwentner, W. Böhmer, J. Chem. Phys. **85**, 2472 (1986)
27. S. Jimenez, A. Pasquarello, R. Car, M. Chergui, Chem. Phys. **233**, 343 (1998)
28. S. Jimenez, M. Chergui, G. Rojas, J. Rubayo. J. Chem. Phys. **114**, 5264 (2001)
29. F. Vigliotti, L. Bonacina, M. Chergui, G. Rojas, J. Rubayo, Chem. Phys. Lett. **362**, 31 (2002)
30. N.W. Ashcroft, N.D. Mermin, *Solid State Physics* (Saunders, Philadelphia, 1976)
31. H.H.W. Thuis, S. Stolte, J. Reuse, J.J.H. van den Biessen. C.J.N. van den Meidenberg, Chem. Phys. **52**, 211 (1980)
32. J.P. Bergsma, P.H. Berens, K.R. Wilson, D.R. Fredkin, E.J. Heller, J. Phys. Chem. **88**, 612 (1984)
33. C. Jeannin, M.-T. Portella-Oberli, S. Jimenez, F. Vigliotti, B. Lang, M. Chergui, Chem. Phys. Lett. **316**, 51 (2000)